351-year tree ring reconstruction of the Gongga Mountains winter minimum temperature and its relationship with the Atlantic Multidecadal Oscillation

Jingxian Li[1] · Jinbao Li[1,2] · Teng Li[3] · Tsun Fung Au[4]

Abstract

Scarcity of high-resolution proxy records has hindered our understanding of long-term climate variations and their mechanism in climate-sensitive regions such as the Tibetan Plateau (TP). In this study, we present a winter minimum temperature (Tmin) reconstruction for the past 351 years (1648–1998) based on a composite tree ring width chronology from three upper treeline sites in the Gongga Mountains, southeastern TP. Despite a loss of sensitivity to winter Tmin after the 1990s, tree growth agrees well with previous December to current March (pDec-cMar) Tmin during 1953–1998, and a regression model based on climate-tree growth relationship over this period explains 52% of the instrumental Tmin variance. The resulting reconstruction exhibits three major cold (1670–1745, 1805–1853, and 1877–1949) and four major warm (1648–1669, 1746–1804, 1854–1876, and 1950–1998) periods over the past four centuries. Long-term winter Tmin variations in the Gongga Mountains have high coherence with those represented by temperature reconstructions in the nearby regions. Together, they indicate close association of the reconstructed warm/cold periods with the positive/negative phases of the Atlantic Multidecadal Oscillation (AMO), suggesting that the AMO may have been a key driving force affecting regional climate over the past few centuries.

This article is part of the topical collection on "Historical and recent change in extreme climate over East Asia," edited by Guoyu Ren, Danny Harvey, Johnny Chan, Hisayuki Kubota, Zhongshi Zhang, and Jinbao Li.

✉   Jingxian Li
    jingxian@connect.hku.hk

[1]   Department of Geography, The University of Hong Kong, Hong Kong SAR, China

[2]   HKU Shenzhen Institute of Research and Innovation, Shenzhen 518057, China

[3]   School of Geography and Remote Sensing, Guangzhou University, Guangzhou 510006, China

[4]   Department of Geography, Indiana University, Bloomington 47405, USA

1 Introduction

The Tibetan Plateau (TP), with an area of about 2.5×10^6 km^2 and an average elevation exceeding 4000 m above sea level (a.s.l.), is essential to atmospheric circulation and hydrological cycle at regional to global scales (Ding 1992). Meteorological data since the 1950s show that the TP has a warming rate that is twice as high as the global average (Chen et al. 2015). However, the sparsity of meteorological stations and the shortness of climate records have prevented scientists from perceiving the mechanism of long-term climate change and the prominence of the anthropogenic warming on the TP (Yao et al. 2019). The state-of-the-art climate models also show limited capacity in simulating temperature and precipitation on the TP (Bothe et al. 2011; Duan et al. 2013). Proxy-based climate studies have therefore been necessary in order to reveal long-term climate variations.

Tree rings have been widely used as a proxy to investigate the climate-growth relationship and to reconstruct paleoclimate owning to their abundant resources, annual resolution, accurate dating, and high sensitivity to climate (Fritts 1976). During the past two decades, a large number of tree ring chronologies have been developed on the southern and eastern TP, many of them have been used to reconstruct long-term changes in regional temperature, precipitation or moisture conditions (e.g. Wang et al. 2014; Shi et al. 2017; Liu et al. 2018; Huang et al. 2019; Li et al. 2020). However, only a few tree ring chronologies are from the Gongga Mountains, the highest barrier on the southeast margin of the TP with the main peak of 7514 m a.s.l. (Chen et al. 2010; Liu et al. 2011). To examine the climate-growth responses and historical temperature variability in this region, two ring width and maximum density chronologies have been developed from the southeastern slope of the Gongga Mountains (Duan et al. 2010a, 2010b). However, the chronologies extended the summer temperature for less than 200 years due to the shortness of the samples. Therefore, there is a need to further expand the tree ring network in order to investigate past temperature change in the Gongga Mountains.

The Atlantic Multidecadal Oscillation (AMO) manifests as the multidecadal alternation between warm and cold phases of North Atlantic sea surface temperature (SST; Muller et al. 2013). It is reported to have an extensive linkage with the climate in different regions around the world, such as temperature fluctuation in Europe, rainfall in North East Brazil and African Sahel, and the Atlantic Hurricanes (Knight et al. 2006; Sutton and Dong 2012). Many previous tree ring studies have revealed that the AMO may have been a key driving force of cold season temperature change on the TP (Wang et al. 2014; Li and Li 2017; Shi et al. 2017; Fang et al. 2019). Nonetheless, there still lacks of proxy records that reveal the long-term AMO influence in the Gongga Mountains.

In this study, we aim to reconstruct winter temperature in the Gongga Mountains through tree ring width chronologies collected from upper treeline sites, which will provide more quantitative information crucial for understanding long-term spatiotemporal temperature change and its forcing mechanism on the southeastern TP.

2 Data and methods

2.1 Study area and climate data

The study sites are located on the southwestern slope of the Gongga Mountains, southeastern TP (Fig. 1, Table 1). The region is under the influence of both East Asian Monsoon and Indian

Monsoon in summer while the westerlies in winter (Ding 1992). It is characterized with chains of deep gorges rising from river valleys (~3000 m a.s.l.) to the main peak of Mount Gongga (7514 m a.s.l.) in short distances. The complex geology and geomorphology result in rich biodiversity and preservation of abundant primeval coniferous forests (Zhang et al. 2013; Yu et al. 2017).

Monthly climate data were obtained from the Jiulong meteorological station (29° 00′ N, 101° 30′ E), the nearest to the sampling sites (Fig. 1). The meteorological records from 1953 to 2014 show an annual mean temperature of 9.0 °C, with monthly mean temperature (Tmean) below 10.0 °C and monthly minimum temperature (Tmin) below 0.0 °C in November–March (Fig. 2). July (15.3 °C) and January (1.2 °C) are the warmest and coldest month, respectively. June receives the highest precipitation of 201.3 mm, while the coldest months of December and January receive only 2.3 mm and 2.4 mm precipitation on average. The annual total precipitation is 909.8 mm on average, with merely 25.0 mm from December to March and the majority (96% of the annual precipitation) from April to October. Therefore, the seasonality of temperature and precipitation reflects a typical monsoonal climate in the study area (Wu et al. 2013). The main growing season generally begins in April and ends in October, while the upper treeline sites should experience a tougher climate than that at the Jiulong station due to higher elevation.

The temperature in Jiulong shows a pronounced warming trend during 1953–2014, with Tmin rising more rapidly than Tmean and Tmax and winter temperature increase higher than all other seasons (Fig. 3, Table S1). The linear regression trendline shows that the annual Tmin increased by 1.77 °C from 1953 to 2014, which is faster than Tmean and Tmax that rose 0.96 °C and 0.78 °C in the same period, respectively. Among the four seasons, winter
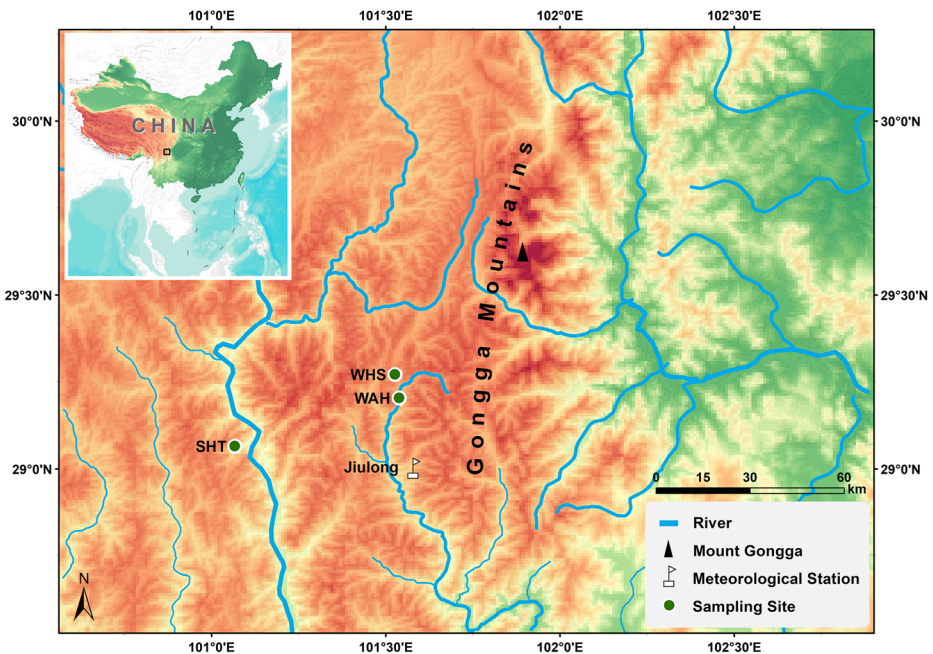

Fig. 1 Map of the Gongga Mountains showing the locations of the sampling sites and the Jiulong meteorological station

Table 1 Site information and tree ring chronology statistics

Site	Location	Elevation (m a.s.l.)	Number (core/tree)	Time span (A.D.)	MSL (year)	SD	MS	AC1	Rbar	EPS	Species
WAH	29° 12′ N, 101° 32′ E	3610	37/19	1638–2014	225	0.54	0.20	0.86	0.54	0.92	*Abies georgei* Orr
WHS	29° 16′ N, 101° 32′ E	3970	58/29	1601–2014	209	0.27	0.20	0.82	0.43	0.94	*Sabina tibetica*
SHT	29° 04′ N, 101° 14′ E	3367	80/43	1569–2014	228	0.56	0.20	0.88	0.55	0.88	*Tsuga chinensis*
JL			175/91	1569–2014	221	0.46	0.20	0.86	0.50	0.96	

MSL mean segment length, *SD* standard deviation, *MS* mean sensitivity, *AC1* first-order autocorrelation, *Rbar* within-trees Rbar, *EPS* expressed population signal
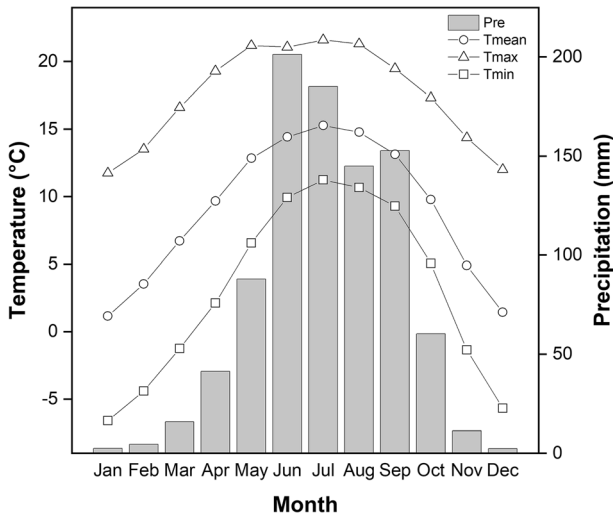
Fig. 2 Monthly Tmax, Tmean, Tmin, and monthly total precipitation at the Jiulong meteorological station over the period 1953–2014

(December–February) temperature has risen more rapidly than other seasons, with winter Tmin rising 2.50 °C whereas summer Tmin for only 1.40 °C (Table S1). Meanwhile, there was no discernible trend for precipitation in any season (Fig. 3).

2.2 Tree ring data

Tree ring samples were taken from three upper treeline sites with the elevation ranging from 3500 m to 4000 m a.s.l., approximately 50–85 km distance from the peak of Mount Gongga (Fig. 1). Among them, 37 cores of *Abies georgei* Orr were sampled from the site WAH, located 20 km north of the Jiulong town; 58 cores of *Sabina tibetica* were sampled from the site WHS, which is located further north at the end of the same valley; 80 cores of *Tsuga chinensis* were sampled at SHT, which is relatively far from the other two sites and 27 km northwest of the Jiulong town.

Tree cores were taken from healthy and relatively isolated trees (no overlap in tree crowns) in order to obtain optimal climate signals. Two cores per tree were drilled from different angles at the breast height. The samples were carefully mounted on slotted wooden slots, air-dried and polished in the lab. Tree ring sequences were crossdated by visually comparing their growth patterns to assign the precise calendar year to each ring. Ring widths were then measured to 0.001 mm precision under microscope with a Velmex measuring system (Velmex Inc., Bloomfield, NY, USA). The quality of visual crossdating was checked statistically with the COFECHA program (Holmes 1983). Cores that were poorly correlated with the master series, either because of age-dependent trend or biological disturbance, were abandoned. One hundred seventy-five increment cores from 91 trees were eventually included to develop three site chronologies and one composite chronology.

To preserve growth variations that reflect climate signals, non-climatic biological trends of the raw ring width series need to be removed through the process of standardization (Fritts 1976). In this study, negative exponential or linear regression curves of any slope were fitted to detrend most series by applying the "signal-free" method (Melvin and Briffa 2008). The cubic
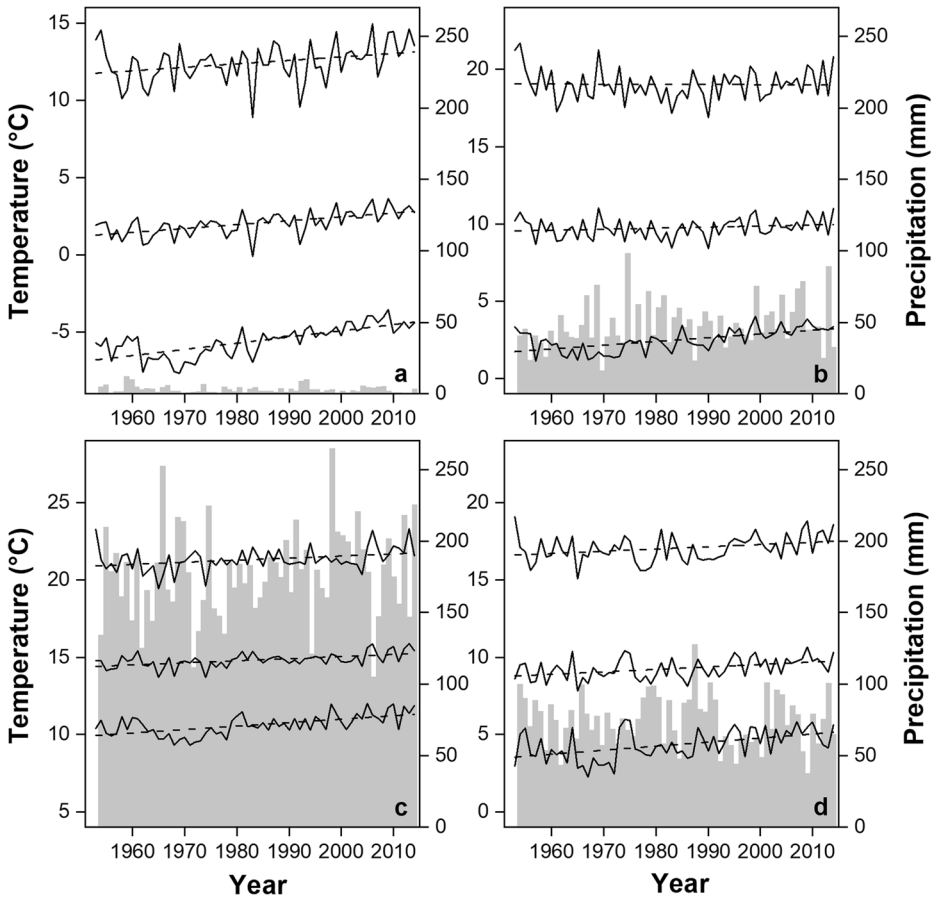
Fig. 3 Seasonal Tmax, Tmean, and Tmin (solid curves) and seasonal total precipitation (shaded bars) at the Jiulong meteorological station over the period 1953–2014 ((a) December–February, (b) March–May, (c) June–August, (d) September–November)

smoothing splines were used to detrend a few series when negative exponential or linear regression curves failed. The tree ring indices were calculated as ratios of raw measurements to the fitted curves (Cook and Peters 1997). Tree ring sequences from each site were merged to build site chronology with a biweight robust mean method, with the variance stabilized through the Rbar weighted method (Frank et al. 2007). The expressed population signal (EPS; Wigley et al. 1984) with a threshold value of 0.85 was applied to determine the reliable span of a chronology, and 30-year running Rbar was calculated to measure the average correlation among ring width series (Cook and Kairiukstis 1990). Other descriptive parameters, including standard deviation (SD), mean sensitivity (MS), and first-order autocorrelation (AC1), were calculated to reveal the quality of each chronology (Table 1).

2.3 Analytical methods

Pearson's correlations between each chronology and monthly climate parameters and their first-differences over an 18-month window from previous May to current October were

calculated to assess the climate-growth relationship in the region. The correlations were also calculated at seasonal scale to reveal the controlling climate factor on tree growth. The dominant climate factor affecting tree growth was adopted for reconstruction via linear regression. Both mean and variance of the reconstruction were adjusted to match that of the instrumental data during their common period.

Due to the short common period between instrumental data and tree ring chronologies, the leave-one-out cross-validation (LOOCV) method was employed to verify the reliability of the regression model (Michaelsen 1987). Other verification statistics, including the reduction of error (RE), sign test (ST), and product mean test (Pmt), were applied to assess the reliability of the reconstruction.

Twenty-one-year running correlations between climate and tree ring data and their first-differences were calculated to test the time-dependence of climate-growth relationship. A 21-year low-pass Fast Fourier Transformation (FFT) filter was applied to highlight the multidecadal variations of the chronologies and the final reconstruction (Nussbaumer 1981). Spatial correlations were calculated for the Jiulong meteorological data and the reconstruction with the Climatic Research Unit (CRU TS4.03) land temperature and self-calibrating Palmer Drought Severity Index (scPDSI) data sets of 0.5° grid resolution via the KNMI Climate Explorer (http://climexp.knmi.nl/) to show their spatial representativeness (van der Schrier et al. 2013; Harris et al. 2014).

3 Results

3.1 Climate-growth relationships

Figure 4 shows the ring width chronologies developed in this study and their sample depths. The ring width chronology covers 377 years (1638–2014) for WAH, 414 years
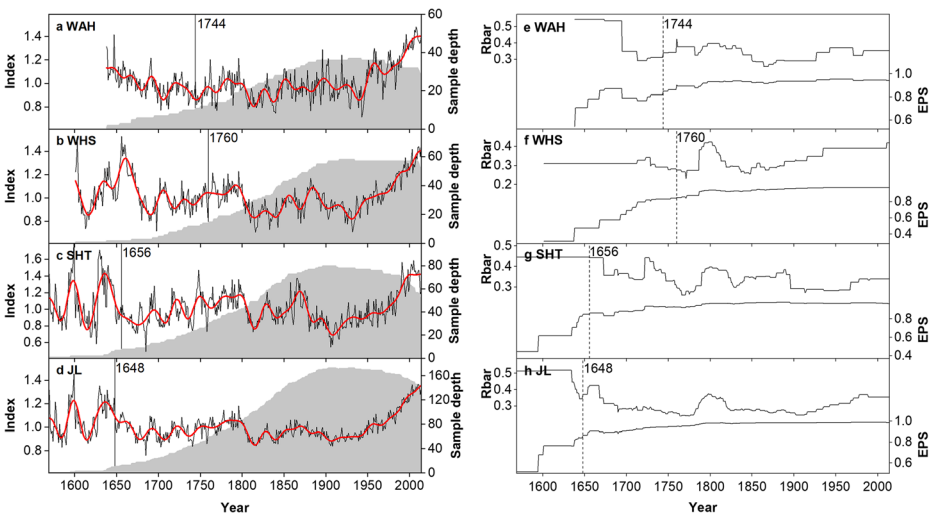

Fig. 4 Tree ring width chronologies from (a) WAH, (b) WHS, (c) SHT, and (d) JL (black curve), the 21-year low-pass FFT filter (red curve), and their corresponding sample depth (shaded area), Rbar, and EPS value (e, f, g, and h). The vertical lines denote the year that the EPS value equals to 0.85
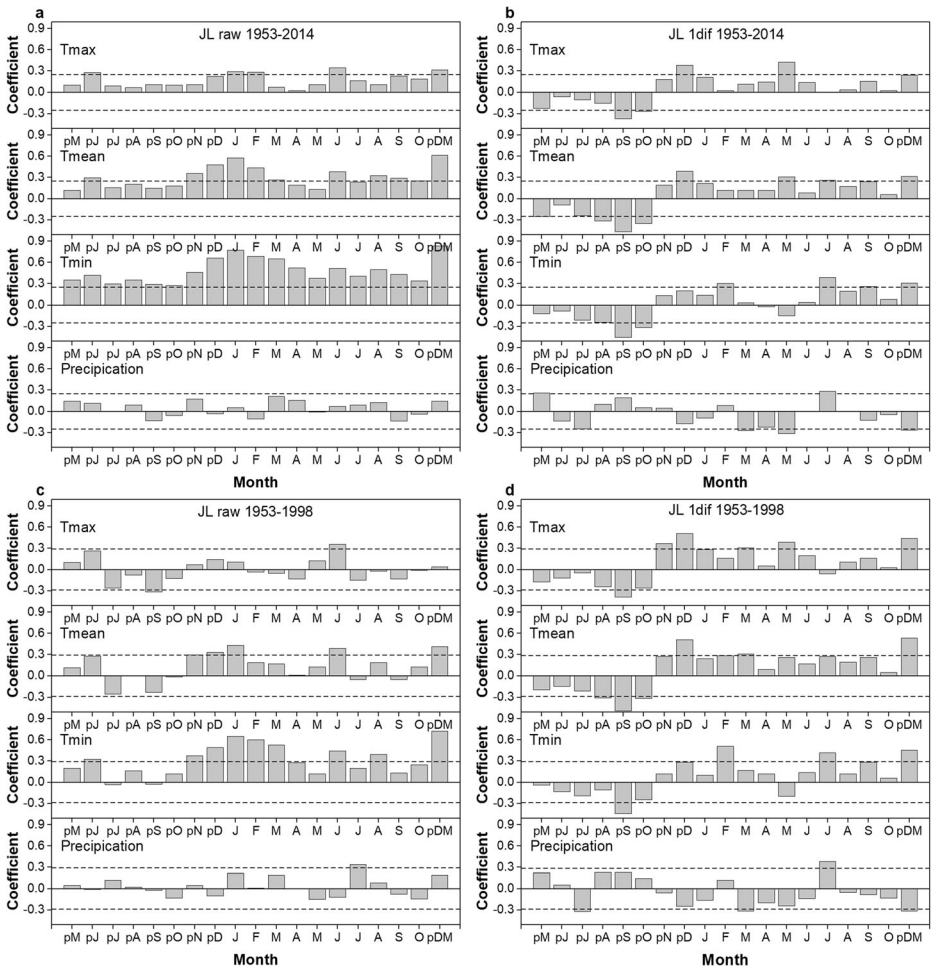
Fig. 5 Raw ((a) and (c)) and first-differenced ((b) and (d)) correlation coefficients of the JL chronology with monthly (previous May to current October) and pDec-cMar climate data (Tmean, Tmin, Tmax, and Precipitation) during 1953–2014 ((a) and (b)) and 1953–1998 ((c) and (d)). The horizontal dash lines denote the 95% confidence level

(1601–2014) for WHS, and 446 years (1569–2014) for SHT (Table 1). Because of their high similarity in annual to decadal variations and also high cross-correlations (WAH:WHS $r = 0.574$; WAH:SHT $r = 0.542$; WHS:SHT $r = 0.420$, $p < 0.001$), the three site chronologies were merged to develop one composite chronology (hereafter named as JL) to minimize the site-specific anomalies and enhance the common variations. Based on the EPS cutoff value of 0.85, the reliable period of the JL chronology spans from 1648 to 2014, with at least 11 cores (Fig. 4). Rbar ranges from 0.237 to 0.519, with the mean value equal to 0.336 (Fig. 4). The standard deviation (SD) and mean sensitivity (MS) of the JL chronology are 0.46 and 0.20, respectively (Table 1). The first-order autocorrelation (AC1) is 0.86, and the overall EPS of the chronology is above 0.96 (Table 1, Fig. 4). The mean segment length (MSL) of the cores is 221 years

Table 2 Statistics of the calibration and verification results for the common period 1953–1998

	Full period calibration					Leave-one-out cross-verification (LOOCV)			
Period	R	R^2	R^2_{adj}	F	r	RMSE	RE	ST	Pmt
1953–1998	0.72	0.52	0.51	47.65	0.69	0.22	0.44	36+/10-	3.29
	Full period calibration on first-difference					LOOCV on first-difference			
Period	R	R^2	R^2_{adj}	F	r	RMSE	RE	ST	Pmt
1953–1998	0.46	0.21	0.19	11.39	0.37	0.17	0.14	28+/17-	2.58

R correlation coefficient between the instrumental and tree ring data, F the F statistic for the statistical significance of the regression model, r correlation coefficient between the instrumental data and the leave-one-out-derived estimates, RMSE root mean squared error, RE reduction of error, ST sign test, Pmt product mean test. $p < 0.05$

(Table 1). These statistics together indicate high reliability of the ring width chronology.

The Pearson's correlations were calculated between the JL chronology and climate factors on an 18-month window from previous May to current October (Fig. 5a). As shown, winter Tmin seemed to be the controlling climate factor on tree growth in the region. The correlation with Tmin was stronger than that with Tmean or Tmax in each month. All months of the 18-month window showed significant positive correlations with Tmin, especially in the winter months before the growing season. The average Tmin from previous December to current March (pDec-cMar) showed the highest correlation with the JL chronology ($r = 0.835$, $p < 0.05$). The correlations between monthly precipitation and tree rings, on the other hand, were very low and non-significant, indicating that moisture was not a limiting factor on tree growth.

However, the first-difference data exhibited much weaker correlations between tree rings and temperature (Fig. 5b), implying an unstable year-on-year consistency through time. The 21-year running correlation indicated that the chronology's response to pDec-cMar Tmin remained significantly positive in the late twentieth century but dropped markedly after the 1990s, with the correlations non-significant from 1994 to 2014 (Fig. S2a). Correlations of the first-difference series dropped even more dramatically, from marginally significant positive by the end of the twentieth century to strong negative after 2010 (Fig. S2b). These results indicate that the chronology experienced the loss of sensitivity to prior winter Tmin signal, a manifestation of the so-called divergence problem (D'Arrigo et al. 2007; Li et al. 2020).

Meanwhile, the responses to raw and first-differenced data of the current growing season (Jul-Oct) Tmin strengthened after the 1990s and became significant ($p < 0.05$) after 2003 and 1994, respectively (Fig. S2c, d). The first-differenced data of the previous growing season (pJul-pOct) Tmin exhibited stronger negative correlations after the 1990s, further complicating the climate-growth relationship under recent warming (Fig. S2f). A comparison between raw and first-differenced running correlations indicates that the first-differenced results are always more sensitive than those from raw data (Fig. S2).

In light of the divergence problem, we omitted the most recent 16 years and re-calculated the monthly correlations (Fig. 5c, d). The correlation of the JL chronology with pDec-cMar Tmin was significantly positive for both raw ($r = 0.721$, $p < 0.05$) and first-differenced data ($r = 0.457$, $p < 0.05$) during 1953–1998 (Table 2). These correlations were also significant at the 0.05 level after adjusting the degrees of freedom, indicating that this climate-growth relationship is robust enough for reconstruction.
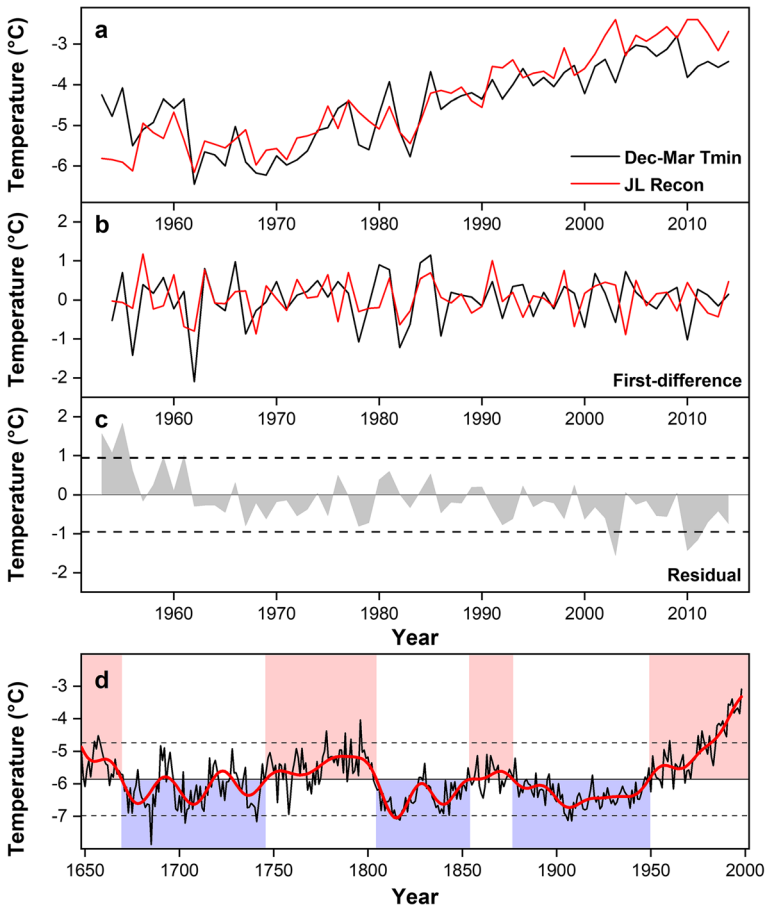
Fig. 6 (a) Comparison of the pDec-cMar Tmin reconstruction (red curve) with the instrumental data (black curve) over the period 1953–2014. (b) Comparison between their first-differences. (c) The residuals of the instrumental minus the reconstructed pDec-cMar Tmin (shaded area). The horizontal dash lines denote the range of ±1 standard deviation. (d) The pDec-cMar Tmin reconstruction from 1648 to 1998 (black curve) and its 21-year low-pass FFT filter (red curve). The solid and dashed horizontal lines denote the mean and the ±1.5 standard deviation of the reconstructed series over 1648–1998, respectively. The red and blue shading highlights the warm and cold phases of the reconstruction

3.2 pDec-cMar Tmin reconstruction

According to the above climate-growth relationship, the pDec-cMar Tmin was reconstructed using a simple linear regression model during the calibration period of 1953–1998. The variance of the reconstruction was adjusted to match that of the instrumental series during their common period. The most recent 16 years were not included due to the loss of response to the Tmin, a method being used in many analogical studies (D'Arrigo et al. 2004; Shi et al. 2017). The reconstruction covers 1648–1998, the period when the chronology's EPS is above 0.85. The reconstruction explains 52% of the instrumental variance, and the F statistic is 47.65 ($p < 0.05$) over the period 1953–1998 (Table 2). Figure 6 shows a comparison between the instrumental and reconstructed pDec-cMar Tmin and their first-differences for visual

inspection. The residuals of the actual minus the estimated data are mostly within the range of ±1 standard deviation (Fig. 6c).

Because the calibration period is not long enough for traditional split-sample calibration and verification tests, the LOOCV method was applied to assess the reliability of the reconstruction model (Michaelsen 1987). The correlation between the instrumental data and the LOOCV derived reconstruction is 0.69 ($p < 0.05$) during the calibration period. The reduction of error (RE = 0.44) and the root mean squared error (RMSE = 0.22) are highly positive, indicating the robustness of the model. Sign test (ST) of both raw and first-differenced series shows a good agreement between the actual and estimated values. The product mean test (Pmt) that measures both sign and magnitude of the departure to the calibration mean is statistically significant, further indicating the validity of the regression model (Fritts 1976). Moreover, the LOOCV approach was used to assess the first-difference of the actual and estimated data, with the correlation remaining significant ($r = 0.37$, $p < 0.05$). All the statistics passed the significance tests successfully (Table 2), confirming the statistical fidelity of the reconstruction model.

The pDec-cMar Tmin was reconstructed for the region over the past 351 years. The mean and standard deviation of the winter Tmin are −5.86 °C and 0.75 °C, respectively. Four major warm periods (1648–1669, 1746–1804, 1854–1876, and 1950–1998) and three major cold periods (1670–1745, 1805–1853, and 1877–1949) were identified with the reconstruction (Fig. 6d). Extreme warm and cold winters were defined when the Tmin exceeded ±1.5 standard deviation interval. Extreme cold winters were identified as in 1685, 1703, 1741, 1815–1817, 1905–1906 and 1908, and extreme warm winters were in 1655, 1657, 1658, 1778, 1788, 1791, 1796, 1960, 1975, 1977–1978, 1981, and all the years after 1985.

4 Discussion

4.1 Physiological processes of the climate-growth relationship

Winter (pDec-cMar) Tmin appears to be the controlling factor of tree growth at our upper treeline sites during the period of 1953–1998. As discussed in our early work, this phenomenon can be explained by several potential physiological processes (Li et al. 2020). For example, an extremely low winter Tmin may form ice crystal that breaks vacuoles, dehydrates cells, and damages the root tissues and tree cambium (Pallardy and Kozlowski 2008). Frozen soil inhibits water absorption and results in winter desiccation, which will reduce tree's potential for future growth (Körner 2012). A colder winter season also signifies a later onset of spring and reduces the length of the growing season in the coming year (Gou et al. 2007), which is supported by a significant positive correlation between winter and spring Tmin at Jiulong station ($r = 0.744$, $p < 0.05$, Table S2). Similar Tmin responses were also reported at many high-altitude sites on the eastern and southeastern TP (Gou et al. 2007; Zhang et al. 2014; Li and Li 2017; Shi et al. 2017; Huang et al. 2019) as well as other parts of China (Duan et al. 2012; Cai et al. 2016), indicating a coherent climate-growth response in similar environments.

4.2 Divergence problem

The above results indicated that a marked divergence phenomenon occurred at our sampling sites under the rapid warming after the 1990s. To ensure that the observed loss of sensitivity

was not caused by the end-effect of detrending methods, we compared the chronology with a new one detrended by fitting the age-dependent spline smoothing curve, and found that the fading responses to the year-to-year variations of winter temperature still exist in spite of the different detrending methods. The manifestation of the divergence phenomenon was identical between various detrending methods, indicating that it was not due to the end-effect of detrending methods.

Tree ring divergence has been widely observed on the eastern and southeastern TP for site-specific causes, including winter drought stress (Shi et al. 2017), increasing cloud cover (Li et al. 2010), winter freezing stress (Li et al. 2012), different elevations, and slope orientations (Guo et al. 2015). However, the divergence at our upper treeline sites demonstrated a marked decline of response to winter Tmin and an enhanced positive response to the growing season temperature under recent warming. Meanwhile, the loss of sensitivity is more prominent in high- rather than low-frequency signals (Fig. S2). Our previous study has discovered and discussed this special manifestation of divergence (Li et al. 2020). As shown, due to the exceeding warming rate of winter than summer temperature (Table S1), winter freezing stress exhibited less control on tree growth, and the upper treeline trees turned to be more constrained by the growing season temperature. Abundant moisture from the summer monsoon facilitates the growth during the growing season, preventing trees from drought stress (Shi et al. 2013; Duan and Zhang 2014; Guo et al. 2015). Since temperature increased rapidly in all seasons (Table S1), trees were still able to capture the overall warming trend but failed to respond to year-to-year climate variability. This explains why the temperature signal remains in low- instead of high-frequency domain. Nonetheless, we note that as the growth divergence occurred rather recently at our sites, further investigations are needed in order to reveal the generality of the phenomenon in the area and other parts of the TP.

4.3 Spatial representativeness of the Tmin reconstruction

Spatial correlations of both observed and reconstructed pDec-cMar Tmin with regional CRU TS4.03 Tmin were calculated over the period 1953–1998. The results show an identical pattern of spatial coherence between our reconstruction and the instrumental data (Fig. 7). Large-scale winter Tmin variation is well captured by our reconstruction, especially in the vast areas of the south and southeastern TP. The same calculation was performed with the CRU scPDSI data, but no significant spatial correlation pattern was found, affirming that tree growth at our sampling sites was not controlled by soil moisture.

To further verify the spatial representativeness of our reconstruction on the TP before the instrumental era, temperature reconstructions from nearby regions were acquired for comparison (Figs. 8 and 9). Four Tmin reconstructions from northern and southeastern TP were obtained, including a 564-year April–March Tmin reconstruction on the east central TP (Li and Li 2017), a winter (November–February) Tmin reconstruction over the period of 1423–2007 on the southeastern TP (Huang et al. 2019), a millennial January–August Tmin reconstruction in the Qilian Mountains of northern TP (Zhang et al. 2014), and an October–April Tmin reconstruction over the past 425 years on the northern TP (Gou et al. 2007). Three Tmean reconstructions from the southeastern TP were also attained for comparison, including a winter (December–February) Tmean reconstruction (1718–2013) in the central Hengduan Mountains (Shi et al. 2017), a millennial annual Tmean reconstruction, and a 449-year April–September Tmean reconstruction in Qamdo area (Duan and Zhang 2014; Wang et al. 2014).

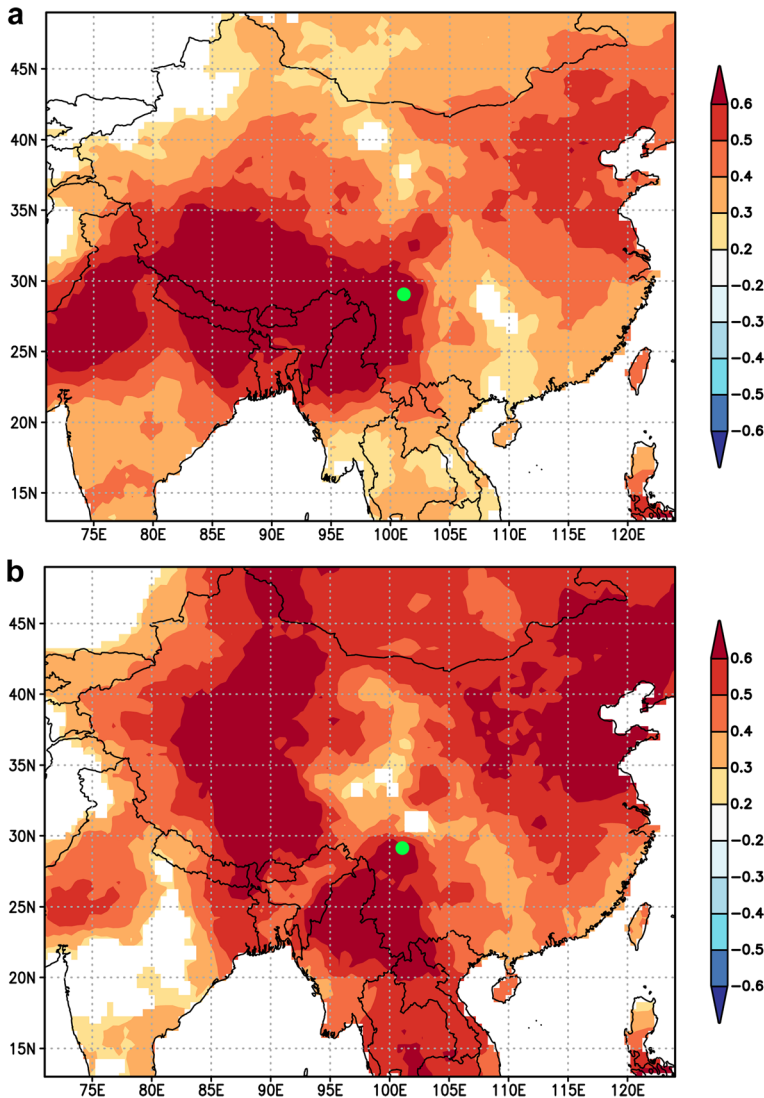**Fig. 7** Spatial correlations of (a) instrumental pDec-cMar Tmin from the Jiulong meteorological station and (b) the JL reconstruction with 0.5° × 0.5° CRU TS4.03 land Tmin during the period 1953–1998. The green dot denotes the location of the study area

Common variations are observed among these reconstructions as shown in Figs. 8 and 9. For example, two cold periods around the 1730s and 1760s were found in most of these series. Two distinct cold episodes during the 1810s–1840s appeared in almost all of the reconstructions, so did the cold epoch in the 1900s–1910s. It is worth noting that the 1815–1817 cold extremes were found in many series, which coincided with the cold events across the Northern Hemisphere (NH) caused by the massive Mount Tambora eruption in 1815. Rapid warming in recent decades was observed in all the records except for the one of Shi et al. (2017), which is mainly because of the existence of the tree ring divergence problem and the shortness of the
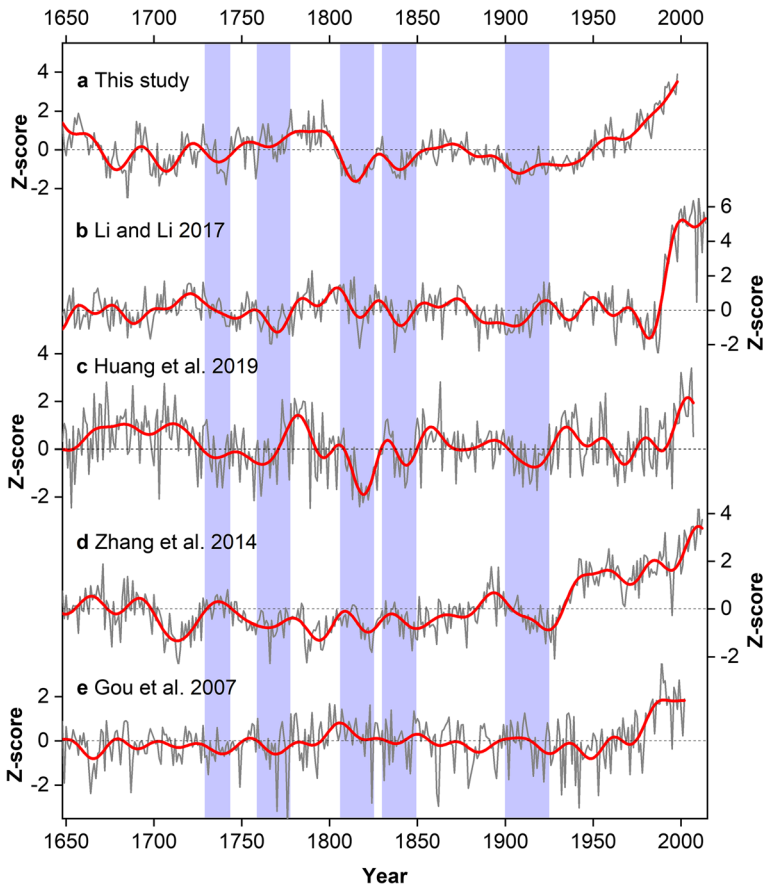
Fig. 8 Comparison of our Tmin reconstruction with the Tmin reconstructions from other studies on the TP. (a) the pDec-cMar Tmin reconstruction of this study; (b) the Apr-Mar Tmin reconstruction on the east central TP (Li and Li 2017); (c) the Nov-Feb Tmin reconstruction on the southeastern TP (Huang et al. 2019); (d) the Jan-Aug Tmin reconstruction in the Qilian Mountains, northern TP (Zhang et al. 2014); and (e) the Oct-Apr Tmin reconstruction on the northeastern TP (Gou et al. 2007). All series were standardized over their common period 1648–1998. The gray thin curves indicate the raw data and red thick curves denote the 21-year low-pass FFT filter. Vertical shadings denote the common cold periods among the records

reconstruction. Nonetheless, there are some inconsistencies among the reconstructions. For example, two cold periods around the 1670s and 1700s in our reconstruction were not evident in some other reconstructions, especially the one of Huang et al. (2019); although in another recent tree ring study (Duan et al. 2019) these two periods were reported cold on the southeastern TP. The cold period during the 1960s–1970s was pronounced in some series but only manifested as a warming pause in others, which could be partly due to the differences in the seasons for reconstruction.

These reconstructions also show a clear geographic categorization, with those located closer to our study (Shao and Fan 1999; Li and Li 2017; Shi et al. 2017) sharing more similarities, while those from the northern TP (Gou et al. 2007; Zhang et al. 2014) and Qamdo (Duan and Zhang 2014; Wang et al. 2014) are less similar to ours. This is probably because different climate systems control the study sites at various locations. The climate in Qamdo is
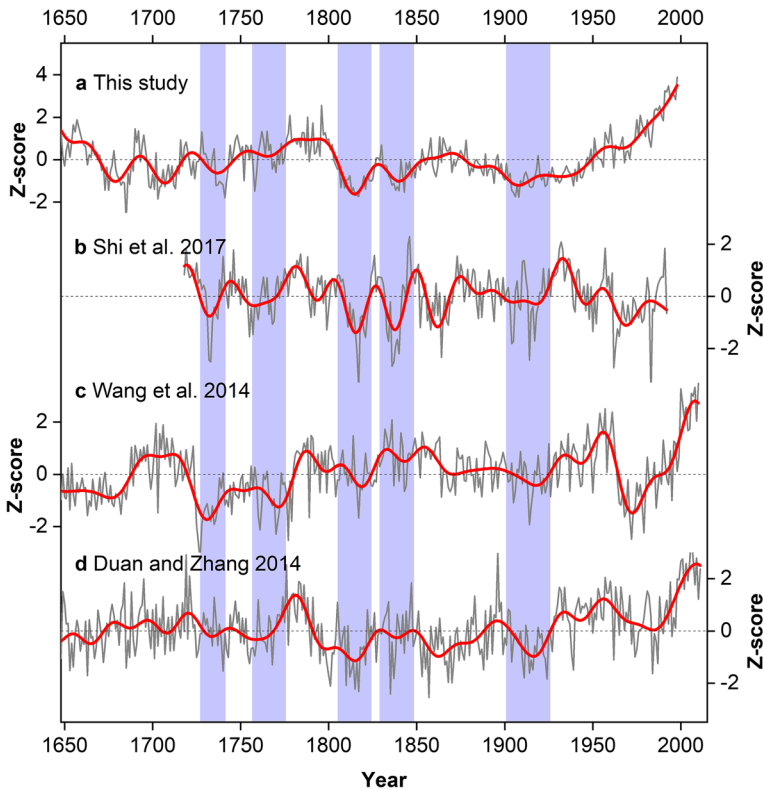
Fig. 9 Comparison of our Tmin reconstruction with the Tmean reconstructions from other studies on the southeastern TP. (a) the pDec-cMar Tmin reconstruction of this study; (b) the Dec-Feb Tmean reconstruction in the central Hengduan Mountains (Shi et al. 2017); (c) the annual Tmean reconstruction in Qamdo (Wang et al. 2014); (d) the Apr-Sep Tmean reconstruction in Qamdo (Duan and Zhang 2014). All series were standardized over their common period 1718–1994. The gray thin curves indicate the raw data and red thick curves denote the 21-year low-pass FFT filter. Vertical shadings denote the common cold periods among the records

dominated by the Indian Monsoon (Duan and Zhang 2014; Wang et al. 2014), while the northern TP sites are mainly influenced by the East Asian Monsoon in summer (Gou et al. 2007; Zhang et al. 2014). Our sites are located in between and may reflect a shift of the impact from the Indian Monsoon to the East Asian Monsoon, which worth investigation in future studies. Besides that, the same cold or warm periods occurred earlier or later, longer or shorter, which highlights marked regional discrepancy in response to the same climate events.

4.4 Association with the AMO

To investigate whether AMO has influenced temperature variation in our study area, one instrumental series and three AMO reconstructions were introduced to conduct correlation analyses with our reconstruction (Kaplan et al. 1998; Mann et al. 2009; Vásquez-Bedoya et al. 2012; Wurtzel et al. 2013). The spatial correlations of the AMO series based on Kaplan et al. (1998) SST index with CRU TS4.03 land Tmin over the period 1953–2014 demonstrated significant positive correlations ($p < 0.01$) from southwest China to north Myanmar, including our study area (Fig. S3). Our Tmin reconstruction agrees well with the warm and cold phases

of the AMO anomalies, with a significant positive correlation of 0.315 ($p < 0.01$) during 1856–1998 (Fig. 10b). Long-term AMO variations can be reflected by a 235-year coral chronology from the Yucatan Peninsula (Vásquez-Bedoya et al. 2012), and a millennial chronology based on Mg/Ca from foraminifera in the Cariaco Basin (Wurtzel et al. 2013). Our reconstruction shows highly synchronized multidecadal warm and cold patterns and is significantly correlated with the two series (Yucatan: $r = 0.359$, $p < 0.01$; Cariaco: $r = 0.387$, $p < 0.01$) as well (Fig. 10c, d). In addition, our reconstruction is also significantly correlated with the decadal-scale AMO reconstruction by Mann et al. (2009) ($r = 0.464$, $p < 0.01$), although the higher correlation may be partly related to the low-frequency nature of the data (Fig. 10e). Nonetheless, these results indicate that the fluctuations of winter Tmin in the Gongga Mountains are largely concurrent with the warm and cold phases of the AMO over the past four centuries.

The relationship between the AMO and temperature change in China has been explored in many studies. The AMO may enhance or weaken air circulation at the middle and upper troposphere over Eurasia (Wang et al. 2009; Ding et al. 2014). Si and Ding (2016) pointed out that the AMO could induce an atmospheric bridge that causes large-scale atmospheric circulation anomalies in the NH. The North Atlantic cooling could, therefore, result in the
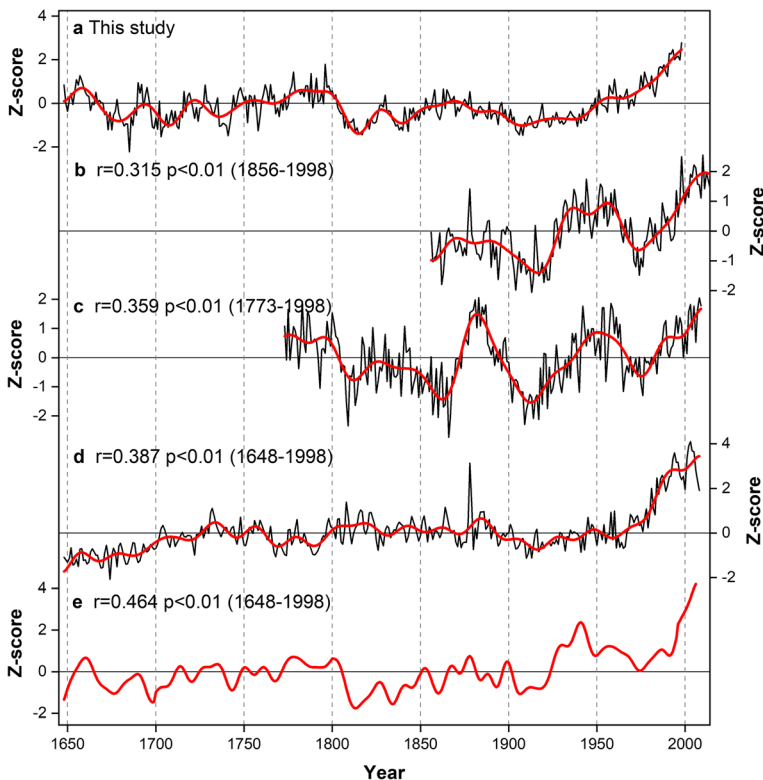

Fig. 10 Comparison of our Tmin reconstruction with the AMO indices. (a) the pDec-cMar Tmin reconstruction of this study; (b) the updated SST-based AMO series from Kaplan et al. (1998); (c) coral-based SST reconstruction at Yucatan Peninsula (Vásquez-Bedoya et al. 2012); (d) foraminifer Mg/Ca-based SST reconstruction at Southern Caribbean (Wurtzel et al. 2013); and (e) decadal AMO reconstruction (Mann et al. 2009). All series were standardized over their own periods. The gray thin curves indicate the raw data and red thick curves denote the 21-year low-pass FFT filter (except for Mann's series). The coefficients indicate the correlation of our Tmin reconstruction with each AMO series over their common periods

shrinking of the East Asian winter monsoon, affecting the southeastern TP (Sutton and Dong 2012). Fang et al. (2019) suggested that the influence of North Atlantic SST on winter temperature of southeastern TP was transported via the southern branch of westerlies separated by the TP, which is supported by the consistent findings of the connection with the AMO from many sites in southwest China and the southern rim of the TP. The Rossby wave propagation (RWP) from the North Atlantic across the Eurasian continent that affects the middle and upper troposphere is suggested as another possible mechanism (Shimizu and Cavalcanti 2011; Grazzini and Vitart 2015). The perturbation of RWP may allow the AMO to implement long-distance influence on temperature anomalies in East Asia (Wang et al. 2013; Wirth et al. 2018). Nonetheless, the mechanism of the connection between the AMO and winter temperature on the southeastern TP could not be fully understood without more knowledge in atmospheric dynamics and modeling.

5 Conclusions

In this study, we developed a composite ring width chronology from three upper treeline sites on the southwestern slope of the Gongga Mountains, southeastern TP. The chronology responded to winter Tmin in general, but a divergence phenomenon was observed since the 1990s as a result of the recent rapid warming. We reconstructed 351 years of pDec-cMar Tmin based on the climate-growth relationship in the calibration period before the divergence (1953–1998), which explains 52% of the instrumental Tmin variance. Four major warm (1648–1669, 1746–1804, 1854–1876, and 1950–1998) and three major cold (1670–1745, 1805–1853, and 1877–1949) periods were identified over the reconstructed period. Spatial correlations and comparisons with other reconstructions further demonstrate coherent temperature variations on the southeastern TP over the past few centuries. Moreover, our reconstruction shows a close linkage with the AMO, with warm (cold) periods coincident with positive (negative) phases of the AMO. Future work should integrate paleoclimate reconstructions with dynamic modeling in order to fully understand the stationarity and mechanism of the AMO influence on climate on the southeastern TP.

References

Bothe O, Fraedrich K, Zhu X (2011) Large-scale circulations and Tibetan Plateau summer drought and wetness in a high-resolution climate model. Int J Climatol 31(6):832–846

Cai Q, Liu Y, Wang Y, Ma Y, Liu H (2016) Recent warming evidence inferred from a tree-ring-based winter-half year minimum temperature reconstruction in northwestern Yichang, South Central China, and its relation to the large-scale circulation anomalies. Int J Biometeorol 60(12):1885–1896

Chen L, Wu F, Liu T, Chen J, Li Z, Pei Z, Zheng H (2010) Soil acidity reconstruction based on tree ring information of a dominant species *Abies fabri* in the subalpine forest ecosystems in southwest China. Environ Pollut 158(10):3219–3224

Chen D, Xu B, Yao T, Guo Z, Cui P, Chen F, Zhang R, Zhang X, Zhang Y, Fan J (2015) Assessment of past, present and future environmental changes on the Tibetan Plateau. Chin Sci Bull 60(32):3025–3035

Cook ER, Kairiukstis LA (1990) Methods of dendrochronology: applications in the environmental sciences. Springer, Berlin

Cook ER, Peters K (1997) Calculating unbiased tree-ring indices for the study of climatic and environmental change. Holocene 7(3):361–370

D'Arrigo RD, Kaufmann RK, Davi N, Jacoby GC, Laskowski C, Myneni RB, Cherubini P (2004) Thresholds for warming-induced growth decline at elevational tree line in the Yukon Territory, Canada. Global Biogeochem Cy 18(GB3021):1–7

D'Arrigo RD, Wilson R, Liepert B, Cherubini P (2007) On the 'divergence problem' in northern forests: a review of the tree-ring evidence and possible causes. Glob Planet Chang 60(3–4):289–305

Ding Y (1992) Effects of the Qinghai-Xizang (Tibetan) plateau on the circulation features over the plateau and its surrounding areas. Adv Atmos Sci 9(1):112–130

Ding Y, Liu Y, Liang S, Ma X, Zhang Y, Si D, Liang P, Song Y (2014) Interdecadal variability of the East Asian Winter Monsoon and its possible links to global climate change. J Meteorol Res 28(5):693–713

Duan J, Zhang Q (2014) A 449 year warm season temperature reconstruction in the southeastern Tibetan Plateau and its relation to solar activity. J Geophys Res-Atmos 119(20):11578–11592

Duan J, Wang L, Li L, Chen K (2010a) Temperature variability since AD 1837 inferred from tree-ring maximum density of *Abies fabri* on Gongga Mountain, China. Chin Sci Bull 55(26):3015–3022

Duan J, Wang L, Xu Y, Sun Y, Chen J (2010b) Response of tree-ring width to climate change at different elevations on the east slope of Gongga Mountains. Geogr Res 29(11):1940–1949

Duan J, Zhang Q, Lv L, Zhang C (2012) Regional-scale winter-spring temperature variability and chilling damage dynamics over the past two centuries in southeastern China. Clim Dynam 39(3–4):919–928

Duan A, Hu J, Xiao Z (2013) The Tibetan Plateau summer monsoon in the CMIP5 simulations. J Clim 26(19): 7747–7766

Duan J, Ma Z, Li L, Zheng Z (2019) August-September temperature variability on the Tibetan Plateau: past, present, and future. J Geophys Res-Atmos 124(12):6057–6068

Fang K, Guo Z, Chen D, Wang L, Dong Z, Zhou F, Zhao Y, Li J, Li Y, Cao X (2019) Interdecadal modulation of the Atlantic Multi-decadal Oscillation (AMO) on southwest China's temperature over the past 250 years. Clim Dynam 52(3–4):2055–2065

Frank D, Esper J, Cook ER (2007) Adjustment for proxy number and coherence in a large-scale temperature reconstruction. Geophys Res Lett 34(16):L16709

Fritts HC (1976) Tree rings and climate. Academic Press, London, New York, San Francisco

Gou X, Chen F, Jacoby G, Cook ER, Yang M, Peng H, Zhang Y (2007) Rapid tree growth with respect to the last 400 years in response to climate warming, northeastern Tibetan Plateau. Int J Climatol 27(11):1497–1503

Grazzini F, Vitart F (2015) Atmospheric predictability and Rossby wave packets. Quart J Roy Meteor Soc 141(692):2793–2802

Guo M, Zhang Y, Wang X, Huang Q, Yang S, Liu S (2015) Effects of abrupt warming on main conifer tree rings in Markang, Sichuan, China. Acta Ecol Sin 35:7464–7474

Harris I, Jones PD, Osborn TJ, Lister DH (2014) Updated high-resolution grids of monthly climatic observations - the CRU TS3.10 dataset. Int J Climatol 34(3):623–642

Holmes RL (1983) Computer-assisted quality control in tree-ring dating and measurement. Tree-Ring Bull 43: 69–78

Huang R, Zhu H, Liang E, Liu B, Shi J, Zhang R, Yuan Y, Grießinger J (2019) A tree ring-based winter temperature reconstruction for the southeastern Tibetan Plateau since 1340 CE. Clim Dynam 53(5–6):3221–3233

Kaplan A, Cane MA, Kushnir Y, Clement AC, Blumenthal MB, Rajagopalan B (1998) Analyses of global sea surface temperature 1856-1991. J Geophys Res-Oceans 103(C9):18567–18589

Knight JR, Folland CK, Scaife AA (2006) Climate impacts of the Atlantic Multidecadal Oscillation. Geophys Res Lett 33(17):L17706

Körner C (2012) Alpine treelines: functional ecology of the global high elevation tree limits. Springer, Berlin

Li T, Li J (2017) A 564-year annual minimum temperature reconstruction for the east central Tibetan Plateau from tree rings. Glob Planet Chang 157:165–173

Li Z, Liu G, Fu B, Zhang Q, Hu C, Luo S (2010) Evaluation of temporal stability in tree growth-climate response in Wolong National Natural Reserve, western Sichuan, China. Chin J Plant Ecol 34(9):1045–1057

Li Z, Liu G, Fu B, Hu C, Luo S, Liu X, He F (2012) Anomalous temperature-growth response of *Abies faxoniana* to sustained freezing stress along elevational gradients in China's western Sichuan Province. Trees 26(4): 1373–1388

Li J, Li J, Li T, Au TF (2020) Tree growth divergence from winter temperature in the Gongga Mountains, southeastern Tibetan Plateau. Asian Geogr 37(1):1–15

Liu X, Zhao L, Chen T, Shao X, Liu Q, Hou S, Qin D, An W (2011) Combined tree-ring width and delta δ^{13}C to reconstruct snowpack depth: a pilot study in the Gongga Mountain, west China. Theor Appl Climatol 103(1–2):133–144

Liu W, Gou X, Li J, Huo Y, Yang M, Lin W (2018) Separating temperature from precipitation signals encoded in tree-ring widths over the past millennium on the northeastern Tibetan Plateau, China. Quaternary Sci Rev 193:159–169

Mann ME, Zhang Z, Rutherford S, Bradley RS, Hughes MK, Shindell D, Ammann C, Faluvegi G, Ni F (2009) Global signatures and dynamical origins of the Little Ice Age and medieval climate anomaly. Sci 326(5957): 1256–1260

Melvin TM, Briffa KR (2008) A "signal-free" approach to dendroclimatic standardisation. Dendrochr 26(2):0–86

Michaelsen J (1987) Cross-validation in statistical climate forecast models. J Clim Appl Meteorol 26(11):1589–1600

Muller RA, Curry J, Groom D, Jacobsen R, Perlmutter S, Rohde R, Rosenfeld A, Wickham C, Wurtele J (2013) Decadal variations in the global atmospheric land temperatures. J Geophys Res-Atmos 118(11):5280–5286

Nussbaumer HJ (1981) Fast Fourier transform and convolution algorithms. Springer, Berlin

Pallardy SG, Kozlowski TT (2008) Physiology of woody plants. Elsevier, Amsterdam, Boston

Shao X, Fan J (1999) Past climate on west Sichuan Plateau as reconstructed from ring-width of dragon spruce. Quat Sci 19(1):81–89

Shi J, Cook ER, Li J, Lu H (2013) Unprecedented January-July warming recorded in a 178-year tree-ring width chronology in the Dabie Mountains, southeastern China. Palaeogeogr Palaeocl 381:92–97

Shi S, Li J, Shi J, Zhao Y, Huang G (2017) Three centuries of winter temperature change on the southeastern Tibetan Plateau and its relationship with the Atlantic Multidecadal Oscillation. Clim Dynam 49(4):1305–1319

Shimizu MH, Cavalcanti IFD (2011) Variability patterns of Rossby wave source. Clim Dynam 37(3–4):441–454

Si D, Ding Y (2016) Oceanic forcings of the interdecadal variability in East Asian summer rainfall. J Clim 29(21):7633–7649

Sutton RT, Dong B (2012) Atlantic Ocean influence on a shift in European climate in the 1990s. Nat Geosci 5(11):788–792

van der Schrier G, Barichivich J, Briffa KR, Jones PD (2013) A scPDSI-based global dataset of dry and wet spells for 1901–2009. J Geophys Res-Atmos 118(10):4025–4048

Vásquez-Bedoya LF, Cohen AL, Oppo DW, Blanchon P (2012) Corals record persistent multidecadal SST variability in the Atlantic Warm Pool since 1775 AD. Paleoceanog 27(3):PA3231

Wang Y, Li S, Luo D (2009) Seasonal response of Asian monsoonal climate to the Atlantic Multidecadal Oscillation. J Geophys Res-Atmos 114(D02112):1–15

Wang J, Yang B, Ljungqvist FC, Zhao Y (2013) The relationship between the Atlantic Multidecadal Oscillation and temperature variability in China during the last millennium. J Quat Sci 28(7):653–658

Wang J, Yang B, Qin C, Kang S, He M, Wang Z (2014) Tree-ring inferred annual mean temperature variations on the southeastern Tibetan Plateau during the last millennium and their relationships with the Atlantic Multidecadal Oscillation. Clim Dynam 43(3–4):627–640

Wigley TML, Briffa KR, Jones PD (1984) On the average value of correlated time-series, with applications in dendroclimatology and hydrometeorology. J Clim Appl Meteorol 23(2):201–213

Wirth V, Riemer M, Chang EK, Martius O (2018) Rossby wave packets on the midlatitude waveguide—a review. Mon Weather Rev 146(7):1965–2001

Wu T, Zhao L, Li R, Wang Q, Xie C, Pang Q (2013) Recent ground surface warming and its effects on permafrost on the central Qinghai-Tibet Plateau. Int J Climatol 33(4):920–930

Wurtzel JB, Black DE, Thunell RC, Peterson LC, Tappa EJ, Rahman S (2013) Mechanisms of southern Caribbean SST variability over the last two millennia. Geophys Res Lett 40(22):5954–5958

Yao T et al (2019) Recent third pole's rapid warming accompanies cryospheric melt and water cycle intensification and interactions between monsoon and environment: multidisciplinary approach with observations, modeling, and analysis. Bull Am Meteor Soc 100(3):423–444

Yu L, Song M, Lei Y, Duan B, Berninger F, Korpelainen H, Niinemets U, Li C (2017) Effects of phosphorus availability on later stages of primary succession in Gongga Mountain glacier retreat area. Environ Exp Bot 141:103–112

Zhang M, Cui Z, Liu G, Chen Y, Nie Z, Fu H (2013) Formation and deformation of subglacial deposits of Hailuogou Glacier in Mt. Gongga, southeastern Tibetan Plateau. J Glaciol Geocryol 35(5):1143–1155

Zhang Y, Shao X, Yin Z, Wang Y (2014) Millennial minimum temperature variations in the Qilian Mountains, China: evidence from tree rings. Clim Past 10(5):1763–1778